Phys. Lett. B 859 (2024) 139101

Contents lists available at ScienceDirect

Physics Letters B

journal homepage: www.elsevier.com/locate/physletb

Letter

The puzzle of suppression of nuclear level density in N ≈ Z Zn isotopes compared to N > Z

Pratap Roy [a,b,*], K. Banerjee [a,b], N. Quang Hung [c,d], N. Ngoc Anh [e], Samir Kundu [a,b], S. Manna [a,b], A. Sen [a,b], T.K. Ghosh [a,b], T.K. Rana [a,b], G. Mukherjee [a,b], R. Pandey [a], S. Mukhopadhyay [a,b], Deepak Pandit [a,b], Debasish Mondal [a], Surajit Pal [a], C. Bhattacharya [a,b]

[a] Variable Energy Cyclotron Centre, 1/AF-Bidhan Nagar, Kolkata-700064, India
[b] Homi Bhabha National Institute (HBNI), Training School Complex, Anushakti Nagar, Mumbai - 400094, India
[c] Institute of Fundamental and Applied Sciences, Duy Tan University, Ho Chi Minh City 700000, Viet Nam
[d] Faculty of Natural Sciences, Duy Tan University, Danang city 550000, Viet Nam
[e] Phenikaa Institute for Advanced Study, PHENIKAA University, Yen Nghia, Ha Dong, Hanoi 12116, Viet Nam

ARTICLE INFO

Editor: H. Gao

Keywords:
Nuclear level density
Neutron evaporation
Isospin effects
TALYS

ABSTRACT

A systematic investigation of isospin dependence of nuclear level density (NLD) is performed for the Zn isotopes. Experimental level densities of ^{67}Zn and ^{61}Zn have been determined by analyzing the spectra of evaporated neutrons emitted from the excited ^{68}Zn and ^{62}Zn nuclei populated via ^{4}He + ^{64}Ni and ^{4}He + ^{58}Ni reactions, respectively. At the low excitation energies, the neutron spectra are predominantly contributed by the first-chance decay, leading to ^{67}Zn and ^{61}Zn as daughters for the two cases. A comparison of the present experimental data along with previously measured NLDs of ^{66}Zn, ^{64}Zn, and ^{60}Zn is performed with state-of-the-art microscopic calculations. While the experimental NLDs of stable isotopes (i.e., ^{67}Zn, ^{66}Zn, and ^{64}Zn) align excellently with theoretical predictions, a compelling contrast emerges for the unstable isotopes ^{61}Zn and ^{60}Zn, exhibiting NLDs an order of magnitude lower than predicted. The possible origins of the observed suppression of NLDs for the N ≈ Z isotopes are discussed. A significant reduction of level density for nuclei situated away from the stability line could have critical implications for the calculation of astrophysical reaction rates pertinent to heavy-element nucleosynthesis.

The nuclear level density (NLD) is a measure of the available quantum levels at a given excitation energy (E), spin (J), and parity (π), and is defined as:

$$\rho(E,J,\pi) = \frac{\Delta N(E,J,\pi)}{\Delta E}, \tag{1}$$

where ΔN is the number of levels within the energy bin ΔE. The total level density is obtained by summing over all spin and parity states:

$$\rho(E) = \sum_{J,\pi} \rho(E,J,\pi). \tag{2}$$

Experimental information on $\rho(E)$ is pivotal in several related areas of physics. NLDs strongly affect neutron-, and proton-capture rates relevant to the heavy-element nucleosynthesis [1,2]. Besides, a precise determination of NLD is useful for many practical applications, such as reactor simulation [3] and production yield estimation of radioisotopes for medical purposes [4]. Apart from being a critical input in nuclear reaction calculations, NLD is of fundamental interest as it can provide stringent tests to microscopic models of nuclear structure and furnish crucial information on the statistical and thermal properties of atomic nuclei [5–8].

In recent times, interest in NLD studies has surged, resulting in several intriguing observations and ideas in the field [9–15]. One of the major issues in this area that remains highly contentious is the isospin dependence of NLD. Isospin, or $n-p$ asymmetry effects in NLD, are expected to be small for nuclei at the valley of stability; however, they can be profound for nuclei situated far away from the stability line. The investigations by Al Quraishi et al. [16,17] suggested that the level densities of neutron- or proton-rich nuclei relevant to the *r*- and *rp*-process may differ from those of neighboring stable nuclei. The nuclear structure looks quite different as one moves several steps away from stability into the neutron- or proton- rich regions. Here, the limits on the

* Corresponding author at: Variable Energy Cyclotron Centre, 1/AF-Bidhan Nagar, Kolkata-700064, India.
E-mail address: roypratap@vecc.gov.in (P. Roy).

https://doi.org/10.1016/j.physletb.2024.139101
Received 29 May 2024; Received in revised form 24 October 2024; Accepted 25 October 2024
Available online 29 October 2024

single-particle states [16], changes in the shell structure [18] and other similar effects could play important roles in modifying the level densities from expected. Al Quraishi et al. [16,17] showed that some of these effects can be taken care of by a parametrization of the level density parameter (a), which reduces its value as the proton number changes from its β-stable value for a given mass number (A) [16]. However, the issue remains debatable due to disparity among different results. Notably, in the investigation of evaporation residue and accompanying light particles around $A \approx 160$, Charity et al. [19] did not observe any evidence of the $n-p$ asymmetry dependence in the level density parameter. The theoretical study of Charity and Sobotka [20] also suggested very little dependence of the level density parameter on neutron or proton richness of the nucleus. However, in our recent studies of neutron evaporation spectra for nuclei around $A = 115$, clear signatures of a reduction of the level density parameter away from the β-stability line are observed [12,21]. Similar trends have also been reported in a few other low-energy particle evaporation studies [22–25]. On the other hand, the recent measurement of level density employing the β-Oslo technique [15] in combination with the "Shape method" [26] suggested that for the short-lived ^{88}Kr the NLD is notably higher compared to the RIPL3 recommended values based on Hartree-Fock Bogoliubov calculations, however, the data agreed reasonably well with other semi-microscopic level density models [27].

A notable decrease in level density for nuclei that are either proton- or neutron-rich could impact nucleosynthesis calculations, particularly those involving (p,γ) or (n,γ) reaction channels. A substantial reduction in NLD as indicated in Refs. [12,21–25], would likely to impede repeated captures, alter the balance between β decay and capture, and ultimately push the paths for rp- and r-process nucleosynthesis closer to the valley of stability. However, drawing definitive conclusions necessitates a thorough examination to ascertain whether the indicated $n-p$ asymmetry dependence of NLD is a general characteristic or specific to a certain mass region. Therefore, systematic investigations into the isospin dependence of NLD across different nuclear mass regions are imperative.

Motivated by the aforementioned considerations, this letter reports an experimental study on the $n-p$ asymmetry dependence of nuclear level density within the Zn isotopes. Experimental level densities of ^{67}Zn and ^{61}Zn were determined by analyzing neutron evaporation spectra from the ^{68}Zn and ^{62}Zn compound nuclei populated through the ^{4}He + ^{64}Ni and ^{4}He + ^{58}Ni reactions, respectively. These results are compared with previously measured NLDs of ^{66,64}Zn [28] and ^{60}Zn [29]. Furthermore, microscopic calculations using the "Exact Pairing plus Independent Particle Model" (EP+IPM) [30,31] were performed for a comprehensive understanding of the experimental data across the Z = 30 isotopic chain, providing crucial insights into the puzzle of isospin dependence in NLD. The experimental level densities could also serve as key inputs in the calculation of capture cross-sections having astrophysical interest in the nucleosynthesis path from Fe to Ge [32] where the Zn isotopes play important role.

The experiment was performed using ^{4}He-ion beams with energies of E_{lab} = 28 and 40 MeV, from the K130 cyclotron at VECC, Kolkata, India. Self-supporting, isotopically-enriched foils of ^{64}Ni ($\approx$ 450 μg/cm^2) and ^{58}Ni ($\approx$ 500 μg/cm^2) were used as targets. The compound nuclei ^{68}Zn and ^{62}Zn were populated in an excitation energy range of $\approx$ 29 - 42 MeV. Eight cylindrical liquid scintillator-based neutron detectors (5-inch × 5-inch) were positioned at laboratory angles (θ_{lab}) of 35°, 55°, 75°, 90°, 105°, 120°, 140°, and 155°, at a distance of 1.5 m from the target. Neutron kinetic energies were determined via the time-of-flight (TOF) method, with the start trigger generated from the prompt γ-rays detected by a 50-element BaF_2 detector array placed near the target. The prompt γ-γ peak in the TOF spectrum served as the time reference. The efficiencies of the neutron detectors were measured under the in-beam conditions using a ^{252}Cf source placed at the target position. Neutron-γ discrimination was accomplished using both TOF and pulse shape measurements [33]. The presence of scattered neutrons in the measured neutron spectra was estimated and subtracted using the "shadow bar" technique [34]. The shadow bar consisted of 40-cm-thick high-density plastic (HDP) and 6-cm Pb blocks was placed in between the target and the detectors. This stops the neutrons coming from the target and only the scattered neutrons could reach up to the detector. The background-corrected neutron spectra measured at various laboratory angles were transformed into the compound nucleus center-of-mass (c.m.) frame using the standard Jacobian transformation.

The measurement of NLD through the analysis of particle evaporation spectra is an established and widely used technique [5,12–14,24,25,35–37]; however, the accuracy of results depend on minimizing the contribution of non-statistical components in the spectra. These components, such as pre-equilibrium emissions, become significant at high bombarding energies ($\gtrsim$ 10 MeV/A). In the present case, such contributions are expected to be small [38,39], particularly at the backward angles. To confirm this, we analyzed the neutron spectra at the forwardmost (35°) and backwardmost (155°) angles using the TALYS (v 1.9) code [40], including both pre-equilibrium (PE) and compound nuclear (CN) contributions in the spectra. The pre-equilibrium calculations were performed with the Exciton model [41] using default parametrization in TALYS [40]. Fig. 1 shows that the pre-equilibrium component is noticeable at the forward angle, where the experimental spectra exhibit enhanced high-energy yields compared to compound nuclear emission. At E_{lab} = 40 MeV, the experimental spectrum at 35° aligns closely with TALYS predictions incorporating both PE and CN components. However, at E_{lab} = 28 MeV, the PE component is slightly overestimated. Conversely, the spectra at 155° for both energies show minimal influence from non-equilibrium components, indicating that these spectra can be adequately explained by the compound nuclear contribution alone [Fig. 1(b) & (d)]. Consequently, we used the backward-angle spectra at the lowest bombarding energy (28 MeV) to determine the NLDs. The experimental spectra at 155° for the two reactions were compared with statistical Hauser-Feshbach (HF) calculations performed using TALYS. For the NLD, the back-shifted Fermi gas (BSFG) formulation [42] given by

$$\rho(E) = \frac{1}{12\sqrt{2}\sigma}\frac{\exp\left[2\sqrt{a(E-\Delta)}\right]}{a^{1/4}(E-\Delta)^{5/4}}, \tag{3}$$

was used as inputs of the TALYS calculations. Here E is the excitation energy, Δ is the pairing energy shift [43], σ is the spin cut-off factor, and a is the level density parameter (LDP). The shell effect in NLD was incorporated using an energy and shell-correction dependent parametrization of the LDP [44]

$$a(U) = \tilde{a}\left[1 + \frac{\Delta S}{U}\{1 - \exp(-\gamma U)\}\right] \tag{4}$$

where, $U = E - \Delta$, and $\tilde{a}$ is the asymptotic value of the LDP obtained in absence of any shell effect. Here ΔS is the ground state shell correction, and γ determines the rate at which the shell effect is depleted with the increase in excitation energy [40]. The asymptotic value of the LDP was approximated as $\tilde{a} = \alpha A$, where A is the mass number, and α is an adjustable parameter, which was tuned to match the experimental data with model calculations. The optical model parameters required to calculate the transmission coefficients, were taken from systematics [40]. The optimum values of α were obtained by fitting the experimental neutron spectra using the χ^2-minimization technique.

The experimental neutron spectra for the ^{4}He + ^{64}Ni and ^{4}He + ^{58}Ni reactions, along with the optimally fitted TALYS predictions, are shown in Fig. 2. For both reactions, the neutron spectra at the present excitation energies are predominantly determined by the first-chance ($1n$) neutron emission leading to ^{67}Zn and ^{61}Zn in respective cases. The contributions of the $1n$ channel are displayed separately by the blue dashed lines in Fig. 2. For neutron energies beyond $\approx$ 6 MeV, any contribution other than the $1n$ channel is negligible. The best-fit values of α are 0.116 ± 0.007 and 0.101 ± 0.006 for the ^{4}He + ^{64}Ni and ^{4}He + ^{58}Ni reactions, respectively. Interestingly, the fitted value of α

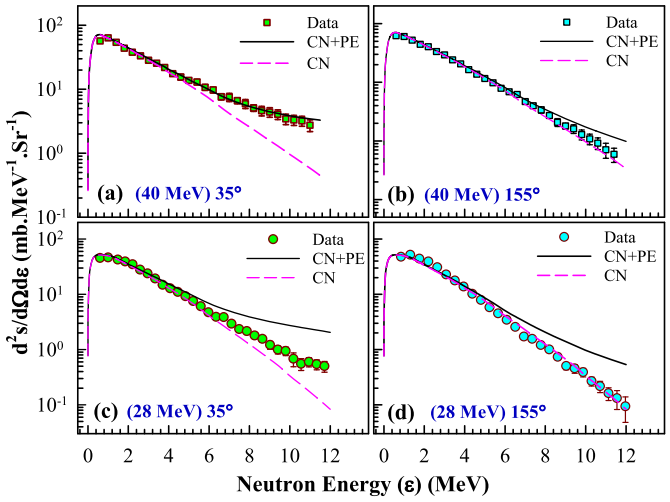

Fig. 1. Experimental double differential cross-section (symbols) of neutrons for the ^{4}He + ^{64}Ni reaction measured at 35° and 155° for the incident energies of (a)-(b) 40 MeV and (c)-(d) 28 MeV. Continuous lines are the predictions of TALYS including contributions from both pre-equilibrium (PE) and compound nuclear (CN) components. The dashed lines represent the CN component alone.

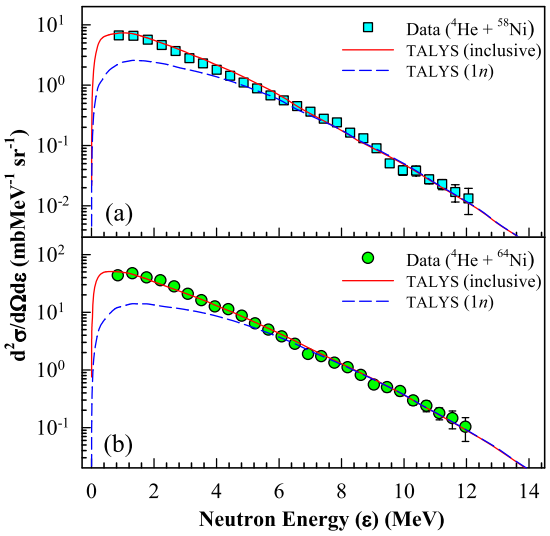

Fig. 2. Experimental neutron spectra at E_{lab} = 28 MeV and θ_{lab} = 155° for the (a) ^{4}He + ^{58}Ni reactions (filled squares) and (b) ^{4}He + ^{64}Ni (filled circles). The optimally fitted TALYS predictions (inclusive) are shown by red continuous lines. The contributions of the 1n channel are represented by blue dashed lines.

for the ^{4}He + ^{64}Ni reaction leading to the β-stable ^{67}Zn, agrees with the systematics value ($\approx$ 0.12) in this mass region [40]; however, it is lower in case of the ^{4}He + ^{58}Ni reaction leading to the neutron-deficient ^{61}Zn. This contrasting behavior hints towards the dependence of the level density parameter on the specific (N, Z) isotopic content of the nucleus.

The experimental neutron spectra in the range of $\approx$ 6 - 12 MeV were further utilized to extract "experimental" level densities $\rho_{exp}(E)$ using the following expression [45,46]:

$$\rho_{exp}(E) = \rho_{model}(E)\frac{(d\sigma/d\varepsilon)_{exp}}{(d\sigma/d\varepsilon)_{model}} \quad (5)$$

Here, $(d\sigma/d\varepsilon)_{exp}$ is the experimental differential cross-section, and $(d\sigma/d\varepsilon)_{model}$ is the differential cross-section calculated by the HF calculation using $\rho(E)_{model}$ as its input NLD. The excitation energy of the residual nucleus (E) was calculated using the relation $E = E^* - S_n - \varepsilon$, where E^* is the compound nuclear excitation energy, S_n is the neutron separation energy, and ε is the kinetic energy of the emitted neutron.

The extracted level densities of ^{67}Zn and ^{61}Zn are plotted as a function of excitation energy in Fig. 3. The NLD obtained using Eqn. 5 requires additional normalization [5,28], which was performed for ^{67}Zn at the neutron separation energy (S_n). The level density at S_n, $[\rho(S_n)]$ was obtained from the measured S-wave resonance spacing [49] following the procedure described in Ref. [5]. The extrapolation of normalization point to the region of experimental data was carried out using the back-shifted Fermi gas formulation, presented by the pink dashed lines in Fig. 3(a). In the case of ^{61}Zn, where neutron resonance measurements are unavailable, the normalization was carried out using the information on the number of discrete energy levels at low energies. The cumulative number of levels, as shown by the continuous red line in the inset of Fig. 3(b), was fitted using the constant temperature (CT) formula [47,48], $N(E) = exp\{(E - E_0)/T_0\}$, by adjusting the energy shift E_0 and constant temperature T_0. The extracted values of E_0 and T_0 are -1.80 MeV and 1.36 MeV, respectively. The fit was constrained to energy levels between N_{min} = 7 and N_{max} = 23 (corresponding to an energy range of $\approx$ 1 - 2.5 MeV). These values were taken from TALYS, where they are selected to ensure a smooth transition between the CT level densities and the Fermi gas values at the matching energy. It should be emphasized that the CT model, $[\rho(E) = (1/T_0)exp\{(E - E_0)/T_0\}]$, provides a more accurate description of NLD at low energies compared to the BSFG model. The level densities derived from the CT fit (shown by the red dashed line in Fig. 3(b)) were used to normalize the NLD of

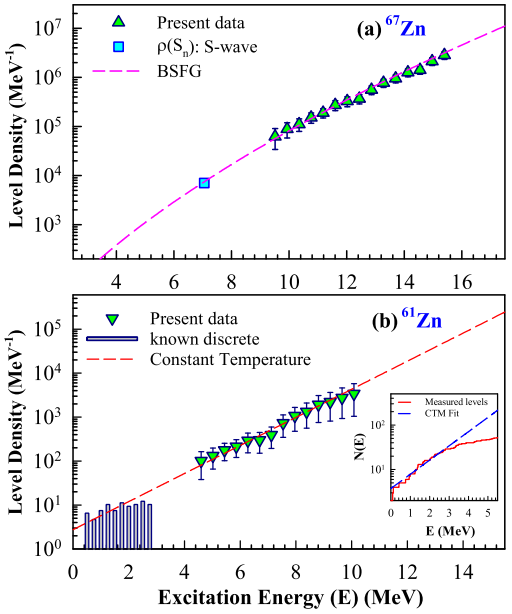

Fig. 3. Experimental level densities (filled triangles) for (a) ^{67}Zn and (b) ^{61}Zn. The pink and red dashed lines represent BSFG and CT predictions, respectively. The cumulative number of energy levels (red continuous line) and corresponding CT fit (blue dashed line) for ^{61}Zn are shown in the inset.

^{61}Zn. The NLD obtained from direct level counting is also displayed by gray vertical bars in Fig. 3(b). It is important to note that the normalization and resulting NLD values depend on the chosen energy window for extracting the CT parameters. To estimate the systematic uncertainty arising from this process, the energy window of the CT fit was shifted by 0.25 MeV in both directions, and the resulting variation in predicted NLD was treated as a systematic uncertainty. It was observed that the uncertainty increases at higher energies, with systematic errors of approximately 68% and 5% at the highest and lowest data points, respectively. These systematic errors were combined in quadrature with the statistical errors.

For a comprehensive understanding of the level densities of the Zn isotopes, microscopic calculations were performed using the state-of-the-art "Exact Pairing plus Independent Particle Model" [30,31]. A key

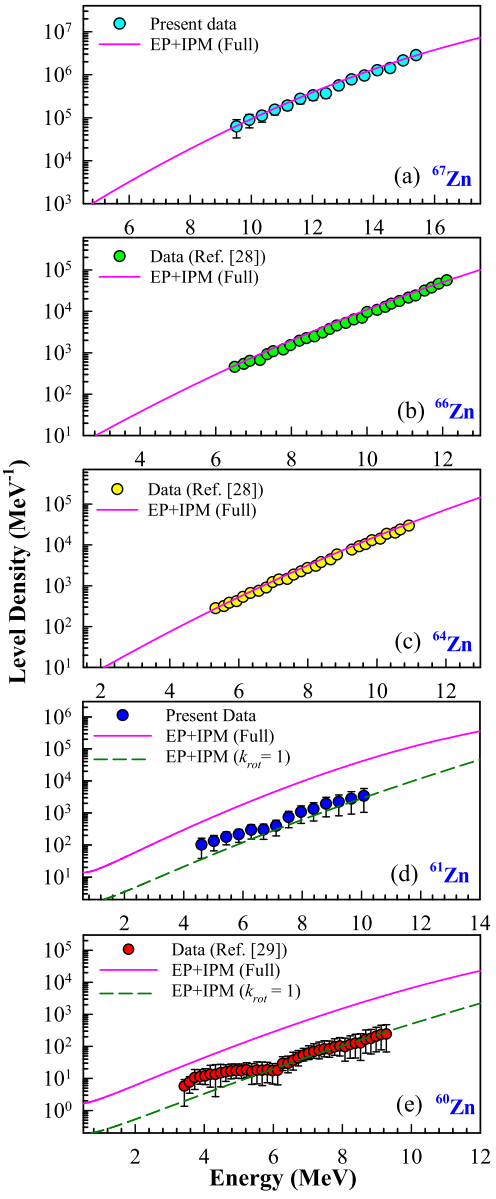

Fig. 4. Comparison of experimental level densities (symbol) with EP+IPM (Full) calculation (pink continuous lines) for (a) ^{67}Zn, (b) ^{66}Zn, (c) ^{64}Zn, (d) ^{61}Zn and (e) ^{60}Zn. The calculations excluding the rotational enhancement factor (k_{rot} = 1) has been shown by the green dashed lines.

feature of EP+IPM is that it incorporates both the thermal and quantal fluctuations in nuclear pairing, which have shown significant effects on NLD [51,52]. Moreover, unlike other regularly used theoretical approaches, the EP+IPM does not employ any adjustable parameter for normalization when compared with experimental data ensuring its microscopic nature. Detailed descriptions of the EP+IPM formalism can be found in references [30,31].

The results from the EP+IPM calculations were directly compared with the present data on ^{67}Zn and ^{61}Zn, as well as with previously measured level densities of ^{66}Zn, ^{64}Zn, and ^{60}Zn [28,29]. Remarkably, the data for stable Zn isotopes- namely ^{67}Zn, ^{66}Zn, and ^{64}Zn align well with the EP+IPM predictions, as shown in Figs. 4(a)-(c). However, the measured level densities of neutron-deficient ^{61}Zn and ^{60}Zn were nearly an order of magnitude lower than the calculated values as seen in Figs. 4(d)-(e). It may be noted that all the Zn isotopes investigated in the present work, exhibit moderate ground-state deformations with the quadrupole deformation parameter $|\beta_2| \approx 0.16$ - 0.18 [50]. For axially deformed nuclei, the collective rotational and vibrational excitations significantly increase the NLD beyond its single-particle estimate. These effects, not included in the pairing Hamiltonian, are incorporated within EP+IPM by using empirical rotational (k_{rot}) and vibrational (k_{vib}) enhancement factors [30]. The EP+IPM calculations performed including these factors are denoted as EP+IPM (Full) and it effectively explains the experimental data for ^{67}Zn, ^{66}Zn, and ^{64}Zn (Fig. 4). Conversely, EP+IPM (Full) overestimates the NLDs of ^{61}Zn and ^{60}Zn by nearly a factor of 10. Interestingly, when setting the rotational enhancement factor k_{rot} to 1, the EP+IPM results align closely with the experimental data for unstable ^{61}Zn and ^{60}Zn (Fig. 4d & 4e). This suggests that these nuclei might behave like spherical or quasi-spherical ones with negligible rotational enhancement, which is puzzling given their non-zero β_2 values as indicated by the finite-range droplet model (FRDM) [50]. For these unstable nuclei, the limit on the single-particle states could also play a decisive role in modifying the NLD [16].

Another crucial factor that could be involved in suppressing the NLD of the N ≈ Z isotopes, compared to others, is the so-called "Wigner" or congruence energy [53–55]. This energy, which depends on $|N - Z|$, originates from the increased overlap of wave functions of particles in identical orbits and provides additional energy stabilization for the N ≈ Z isotopes. In TALYS, the default shell correction ($\Delta S'$) is defined as the difference between the experimental mass and the theoretical mass calculated within the Liquid Drop Model (LDM) using the parametrization of Mengoni and Nakajima [56]. The latter, however, does not include a Wigner term (E_W). As a result, the actual shell correction ΔS should be determined as $\Delta S' - E_W$.

For a quantitative understanding, we evaluated E_W for the present set of Zn isotopes using a semi-microscopic model following the prescription of Ref. [54],

$$E_W = V_W exp\left\{-\lambda\left(\frac{N-Z}{A}\right)^2\right\} + V'_W|N-Z|exp\left\{-\left(\frac{A}{A_0}\right)^2\right\}. \quad (6)$$

The parameters V_W, V'_W, λ and A_0 were taken from the latest version of BSk26 force [54]. The calculated values of E_W, alongwith ΔS, and $\Delta S'$ are listed in Table 1. Clearly, the cases of interest here, ^{60,61}Zn, have maximal Wigner energies, while for the heavier isotopes this energy stabilization is minimal (Table 1). To illustrate the impact of the Wigner energy on the calculated NLD, Fig. 5 compares the experimental NLDs of ^{60,61}Zn with those predicted using the BSFG model under various scenarios. Since it is unclear if the Wigner energy and the shell effects should fade out in exactly the same way, we decided to treat them independently by modifying Eq. (4) as follows.

$$a(U) = \tilde{a}[1 + \frac{\Delta S}{U}\{1 - \exp(-\gamma_S U)\} + \frac{E_W}{U}\{1 - \exp(-\gamma_W U)\}] \quad (7)$$

with γ_S and γ_W being the rates at which the shell and Wigner energy effects damp, respectively. In addition, in all scenarios, $\tilde{a}$ and γ_S are calculated using global parametrization, i.e., $\tilde{a} = 0.12A$ and $\gamma_S = 0.410289A^{-1/3}$, whereas, the values of all the other parameters are taken from the TALYS default. In the first scenario, we consider the BSFG NLDs with the assumption that both shell correction and Wigner energy have no effect on the calculated NLDs (black solid lines in Fig. 5). This assumption is imposed by setting ΔS and E_W in Eq. (7) to zero. It is shown that the predicted NLDs strongly overestimate the experimental data. In the second scenario, both effects were enabled and assumed to fade-out at the same rate (i.e., $\gamma_S = \gamma_W$), the predictions (red long-dashed lines) showed a significant improvement, coming closer to the experimental data, underscoring the importance of Wigner energy for $N \approx Z$ nuclei. Another two scenarios, in which the Wigner effect is assumed to have the fade-out rates equal to half (i.e., $\gamma_W = 0.5\gamma_S$) and

Table 1
Shell correction and Wigner energies for the different isotopes.

Nucleus	$\Delta S'$ [56] (MeV)	E_W [54] (MeV)	ΔS (MeV)
^{67}Zn	1.846	-0.02	1.866
^{66}Zn	0.797	-0.07	0.864
^{64}Zn	-0.590	-0.40	-0.190
^{61}Zn	-2.920	-1.62	-1.300
^{60}Zn	-4.060	-1.80	-2.260

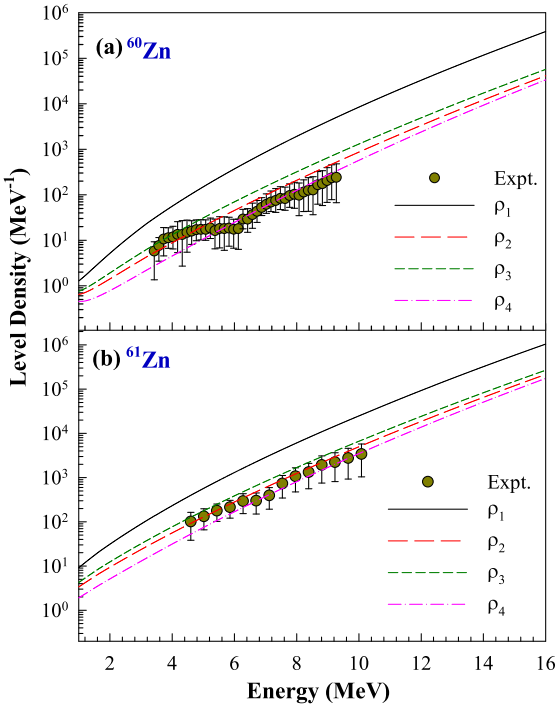

Fig. 5. BSFG level densities with: no structure modification (ρ_1), both shell and Wigner structure effects with the same fade-out rate (ρ_2), and with the Wigner-energy fade-out rate half (ρ_3) and twice (ρ_4) of the shell correction term (see text for details).

twice (i.e., $\gamma_W = 2.0\gamma_S$) that of the shell damping, were also considered. The predictions (green short-dashed and pink dash-dotted lines in Fig. 5) indicates that the calculated NLD changes significantly as the Wigner energy damping rate varies. The experimental data are somewhat better reproduced with higher damping rate of the Wigner energy compared to shell effect. The present analysis brings out the crucial role of Wigner energy and its damping in NLD calculations, that to our knowledge, has not been presented previously.

We have discussed several potential reasons for the observed reduction of NLD in the N ≈ Z isotopes. Another possible origin for the discrepancy between EP+IPM (Full) and the NLD data of ^{60,61}Zn could also be partially due to the neutron-proton (*np*) pairing effect [57], which was not included in the current calculations. Similar to the congruence energy, the *np* pairing could be significant for the N ≈ Z nuclei such as ^{60}Zn and ^{61}Zn. Increased *np* pairing will reduce the level density, as observed in these systems.

The present findings open up new avenues for further investigation to untangle the possible roles of reduced deformation, *np* pairing, congruence, and isospin effects in explaining the observed differences between the NLDs of the stable and unstable Zn isotopes.

To summarize, this study focused on investigating the nuclear level densities of various Zn isotopes by analyzing neutron evaporation spectra within the statistical Hauser-Feshbach approach. The findings revealed that the optimal asymptotic level density parameter $\tilde{a}$ showed good alignment with systematics for the β-stable ^{67}Zn but was significantly lower for the neutron-deficient ^{61}Zn. Additionally, microscopic calculations using the Exact Pairing plus Independent Particle Model were performed and compared with experimental NLDs of ^{67}Zn, ^{66}Zn, ^{64}Zn, ^{61}Zn, and ^{60}Zn. The EP+IPM predictions agreed well with experimental NLDs for stable isotopes but overestimated the experimental data for the unstable isotopes. Intriguingly, experimental NLDs of the unstable isotopes matched reasonably well with the EP+IPM model when excluding the rotational enhancement factor, even though these nuclei had moderate ground-state deformations. The potential reasons for the observed NLD suppression in the N ≈ Z isotopes were discussed, highlighting the important role of the congruence energy. These findings necessitate further theoretical and experimental investigations to elucidate the underlying mechanisms and validate the observed trends across different nuclear mass regions. The results presented here could have important implications for the calculation of astrophysical reaction rates, impacting our understanding of nucleosynthesis processes.

The authors would like to acknowledge the VECC Cyclotron operators for the smooth running of the accelerator during the experiment. We thank J. K. Meena, A. K. Saha, J. K. Sahoo, and R.M. Saha for their help during the experimental setup and Prof. Subinit Roy for providing the ^{64}Ni target. We thankfully acknowledge Prof. Lee Sobotka (of Washington University) for their valuable inputs and suggestions on the normalization and interpretation of the NLD data.

Declaration of competing interest

The authors declare that they have no known competing financial interests or personal relationships that could have appeared to influence the work reported in this paper.

Data availability

Data will be made available on request.

References

[1] A.C. Larsen, A. Spyrou, S.N. Liddick, M. Guttormsen, Prog. Part. Nucl. Phys. 107 (2019) 69–108.
[2] M. Arnould, K. Takahashi, Rep. Prog. Phys. 62 (1999) 395.
[3] C.D. Bowman, Annu. Rev. Nucl. Part. Sci. 48 (1998) 505.
[4] H.R. Mirzaei, et al., J. Cancer Res. Ther. 12 (2016) 520.
[5] Pratap Roy, K. Banerjee, T.K. Rana, et al., Eur. Phys. J. A 57 (2021) 48.
[6] Vu Dong Tran, Nhut Huan Phan, Quang Hung Nguyen, et al., J. Phys. G, Nucl. Part. Phys. 51 (2024) 065105.
[7] Balaram Dey, N. Quang Hung, Deepak Pandit, et al., Phys. Lett. B 789 (2019) 634–638.
[8] F. Giacoppo, F.L. Bello Garrote, L.A. Bernstein, Phys. Rev. C 90 (2014) 054330.
[9] X.F. Jiang, X.H. Wu, P.W. Zhao, J. Meng, Phys. Lett. B 849 (2024) 138448.
[10] S. Hilaire, S. Goriely, S. Peru, G. Gosselin, Phys. Lett. B 843 (2023) 137989.
[11] C. Schmitt, P.N. Nadtochy, K. Mazurek, Phys. Lett. B 840 (2023) 137873.
[12] R. Shil, K. Banerjee, Pratap Roy, et al., Phys. Lett. B 831 (2022) 137145.
[13] T. Santhosh, P.C. Rout, S. Santra, et al., Phys. Lett. B 841 (2023) 137934.
[14] Deepak Pandit, Balaram Dey, Srijit Bhattacharya, et al., Phys. Lett. B 816 (2021) 136173.
[15] A. Spyrou, S.N. Liddick, A.C. Larsen, et al., Phys. Rev. Lett. 113 (2014) 232502.
[16] S.I. Al-Quraishi, S.M. Grimes, T.N. Massey, D.A. Resler, Phys. Rev. C 67 (2003) 015803.
[17] S.I. Al-Quraishi, S.M. Grimes, T.N. Massey, D.A. Resler, Phys. Rev. C 63 (2001) 065803.
[18] T. Otsuka, A. Gade, O. Sorlin, T. Suzuki, Y. Utsuno, Rev. Mod. Phys. 92 (2020) 015002.
[19] R.J. Charity, L.G. Sobotka, J.F. Dempsey, et al., Phys. Rev. C 67 (2003) 044611.
[20] R.J. Charity, L.G. Sobotka, Phys. Rev. C 71 (2005) 024310.
[21] Pratap Roy, K. Banerjee, T.K. Rana, et al., Phys. Rev. C 102 (2020) 061601(R).
[22] G.K. Prajapati, Y.K. Gupta, B.V. John, et al., Phys. Rev. C 102 (2020) 054605.
[23] A. Richter, W. Von Witsch, P. Von Brentano, et al., Phys. Lett. 14 (1965) 121.
[24] B.V. Zhuravlev, A.A. Lychagin, N.N. Titarenko, Phys. At. Nucl. 69 (2006) 363–370.
[25] A.V. Voinov, T. Renstrom, D.L. Bleuel, et al., Phys. Rev. C 99 (2019) 054609.
[26] M. Wiedeking, M. Guttormsen, A.C. Larsen, et al., Phys. Rev. C 104 (2021) 014311.
[27] D. Mucher, A. Spyrou, M. Wiedeking, et al., Phys. Rev. C 107 (2023) L011602.
[28] A.P.D. Ramirez, A.V. Voinov, S.M. Grimes, et al., Phys. Rev. C 88 (2013) 064324.

[29] D. Soltesz, M.A.A. Mamun, A.V. Voinov, et al., Phys. Rev. C 103 (2021) 015802.
[30] N. Quang Hung, N. Dinh Dang, L.T. Quynh Huong, Phys. Rev. Lett. 118 (2017) 022502.
[31] N. Dinh Dang, N. Quang Hung, L.T. Quynh Huong, Phys. Rev. C 96 (2017) 054321.
[32] Saumi Dutta, G. Gangopadhyay, Abhijit Bhattacharyya, Phys. Rev. C 94 (2016) 054611.
[33] Pratap Roy, K. Banerjee, A.K. Saha, et al., Nucl. Instrum. Methods Phys. Res., Sect. A 901 (2018) 198–202.
[34] R. Roy, Study of nuclear level density using particle evaporation as a probe, Ph.D. thesis, HBNI, India, 2017, http://www.hbni.ac.in/phdthesis/phys/PHYS04201304001.pdf.
[35] A.V. Voinov, N. Alanazi, S. Akhtar, et al., Phys. Rev. C 108 (2023) 034302.
[36] T. Santhosh, P.C. Rout, S. Santra, et al., Phys. Rev. C 108 (2023) 044317.
[37] S. Komarov, R.J. Charity, C.J. Chiara, et al., Phys. Rev. C 75 (2007) 064611.
[38] S.M. Grimes, J.D. Anderson, J.W. McClure, et al., Phys. Rev. C 10 (1974) 2373.
[39] R.M. Wood, R.R. Borchers, H.H. Barschall, Nucl. Phys. 71 (1965) 529–545.
[40] A. Koning, S. Hilaire, S. Goriely, Eur. Phys. J. A 59 (2023) 131, online at https://nds.iaea.org/talys/.
[41] A.J. Koning, M.C. Duijvestijn, Nucl. Phys. A 744 (2004) 15–76.
[42] H.A. Bethe, Phys. Rev. 50 (1936) 332, Rev. Mod. Phys. 9 (1937) 69.
[43] W. Dilg, W. Schantl, H. Vonach, M. Uhl, Nucl. Phys. A 217 (1973) 269.
[44] A.V. Ignatyuk, G.N. Smirenkin, A.S. Tishin, Sov. J. Nucl. Phys. 21 (1975) 255.
[45] H. Vonach, Proceedings of the IAEA advisory group meeting on basic and applied problems of nuclear level densities, National Laboratory Report No. BNL-NCS-51694 in: Proceedings of the IAEA Advisory Group Meeting on Basic and Applied Problems of Nuclear Level Densities, Upton, New York, 1983, Brookhaven National Laboratory Report No. BNL-NCS-51694, 1983, p. 247.
[46] A. Wallner, B. Strohmaier, H. Vonach, Phys. Rev. C 51 (1995) 614.
[47] A.J. Koning, S. Hilaire, S. Goriely, Nucl. Phys. A 810 (1) (2008) 13–76.
[48] A. Gilbert, A.G.W. Cameron, Can. J. Phys. 43 (1965) 1446–1496.
[49] R. Capote, M. Herman, P. Oblozinsky, et al., Nucl. Data Sheets 110 (2009) 3107.
[50] P. Moller, A.J. Sierk, T. Ichikawa, H. Sagawac, At. Data Nucl. Data Tables 109–110 (2016) 1.
[51] N. Quang Hung, N. Dinh Dang, Phys. Rev. C 81 (2010) 057302.
[52] N. Quang Hung, N. Dinh Dang, Phys. Rev. C 82 (2010) 044316.
[53] W. Myers, Droplet model of atomic nuclei, LBNL Report#: LBL-5846, Lawrence Berkeley National Laboratory, 1977.
[54] S. Goriely, N. Chamel, J.M. Pearson, Phys. Rev. C 88 (2013) 024308.
[55] L. Buskirk, K. Godbey, W. Nazarewicz, W. Satula, Phys. Rev. C 109 (2024) 044311.
[56] A. Mengoni, Y. Nakajima, J. Nucl. Sci. Technol. 31 (1994) 151.
[57] S. Frauendorf, A.O. Macchiavelli, Prog. Part. Nucl. Phys. 78 (2014) 24–90.